Physica B: Physics of Condensed Matter xxx (2017) 1–4

Contents lists available at ScienceDirect

Physica B: Physics of Condensed Matter

journal homepage: www.elsevier.com/locate/physb

The origin of the polar symmetry in huebnerite-type multiferroics

So-Hyun Park [a,*], David Behal [a,b], Björn Pedersen [b]

[a] Section Crystallography, Department for Earth and Environmental Sciences, Ludwig-Maximilians-Universität München, Munich, Germany
[b] Forschungs-Neutronenquelle Heinz Maier-Leibnitz (FRM II), Technische Universität München, Garching, Germany

ARTICLE INFO

Keywords:
Huebnerite
Multiferroic
Polar symmetry
Helical spin-wave
Neutron diffraction

ABSTRACT

The magnetic structure of the multiferroic phase AF2 of huebnerite ($MnWO_4$) has been re-investigated based on the polar space group ***P***2, instead of ***P***2/*c* widely accepted in literature. The site character between two independent sites for Mn^{2+}, Mn_a and Mn_b, fairly differs from each other in terms of bond valence sums. This hidden intrinsic dipole moment is the true origin of the chiral magnetic order in AF2 in the polar superspace group ***P***2.1′ (α, 1/2, γ)0s. From structure refinements using single crystal neutron diffraction data at 10 K the ellipticity of the spin helix could be determined to be 0.92 and 0.77 at Mn_a and Mn_b, respectively. The different contributions of two chiral spin-textures to electric polarisation microscopically measurable in the ***b*** axis (P_b) could be estimated with P_b (Mn_a) = 22.8 μCm^{-2} and P_b (Mn_b) = 12.2 μCm^{-2}.

1. Introduction

It has been accepted that the multiferroic AF2 phase of $MnWO_4$ exhibits an incommensurably modulated helical spin ordering in the non-polar space group ***P***2/*c* [1–3]. The chiral spin-waves in AF2 are understood by geometrical frustration of the Mn-O-Mn-triangle within the zigzag MnO_6-chains via inverse Dzyaloshinskii-Moriya (*IDM*) interaction competing with interchain isotropic exchange interactions (*IEI*) along the crystallographic ***c*** axis (Fig. 1). A strong spin-orbit coupling can be driven from the contra influence of *IDM* and *IEI* on the spin-spiral orientations at two symmetrically related Mn sites in ***P***2/*c* [2]. This was suggested as the origin of the magnetoelectric (*ME*) coupling inducing electric polarisation of max. ~50 μC/cm^2 at ~7.8 K and zero external fields [2,3]. On the other hand, the so-called Rashba or/and Dresselhaus effects break inversion- or non-polar symmetries by magnetic order at polar or non-inversion atomic sites [4]. Indeed, Mn^{2+} cations (S = 5/2) in $MnWO_4$ are located at such atomic sites, C_2 in both ***P***2/*c* and its direct subgroup ***P***2, allowing strong spin-orbit coupling responsible for improper ferroelectricity. All these suggestions have been considered to explain microscopically measurable electric polarisation in the non-polar arrangement of Mn^{2+} cations in the title compound.

In this context-considering the role of polar Mn^{2+} sites for the *ME* coupling-we have investigated huebnerite [5], as well as (In^{3+}, Na^+, vacancy)-doped $MnWO_4$ solid-solution compounds [6–9]. Surprisingly, results from extensive neutron and X-ray diffraction including Renninger scans pointed to the polar space group ***P***2 true for all those huebnerite-type structures [5–7,10]. There might be weak electric dipole moments in these compounds even in the paramagnetic state because of the presence of two independent polar C_2 sites for Mn^{2+} (denoted as Mn_a and Mn_b). Indeed, this non-inversion property in $MnWO_4$ and In^{3+}-doped $MnWO_4$ crystals could be proven by a week effect of second-harmonic generation [10]. Furthermore, we have found a strong agreement of calculated and observed inelastic neutron scattering spectra of magnon energy from two distinctly spin-canting textures in its commensurately modulated low-temperature phase AF1 using the polar superspace magnetic symmetry ***P***2.1′ (α, 0, γ)0s [11]. In the current report, we present the AF2 structure of huebnerite at 10 K based on the polar space group ***P***2.

2. Experimental

Details of sampling, optical, and chemical information about the investigated huebnerite crystals from Pasto Bueno are found in our previous report [5]. A chemically pure huebnerite crystal was used to collect neutron single crystal diffraction (NSCD) data at 10 K at the instrument RESI in the neutron source facility Heinz Maier-Leibnitz (FRM-II at Garching, Germany) [12]. Applying a wavelength of 1.0481 Å (Cu(422) monochromator) a set of 2D raw data was detected on a MAR345 image plate and processed using the program package EVAL [13]. Relevant experimental parameters of NSCD and the crystal lattice are summarized in Table 1. Using the starting model given in Ref. [5] the nuclear structure was refined by least-squares calculation with the program package

* Corresponding author.
E-mail address: sohyun.park@lmu.de (S.-H. Park).

https://doi.org/10.1016/j.physb.2017.11.034
Received 25 August 2017; Accepted 8 November 2017
Available online xxxx
0921-4526/

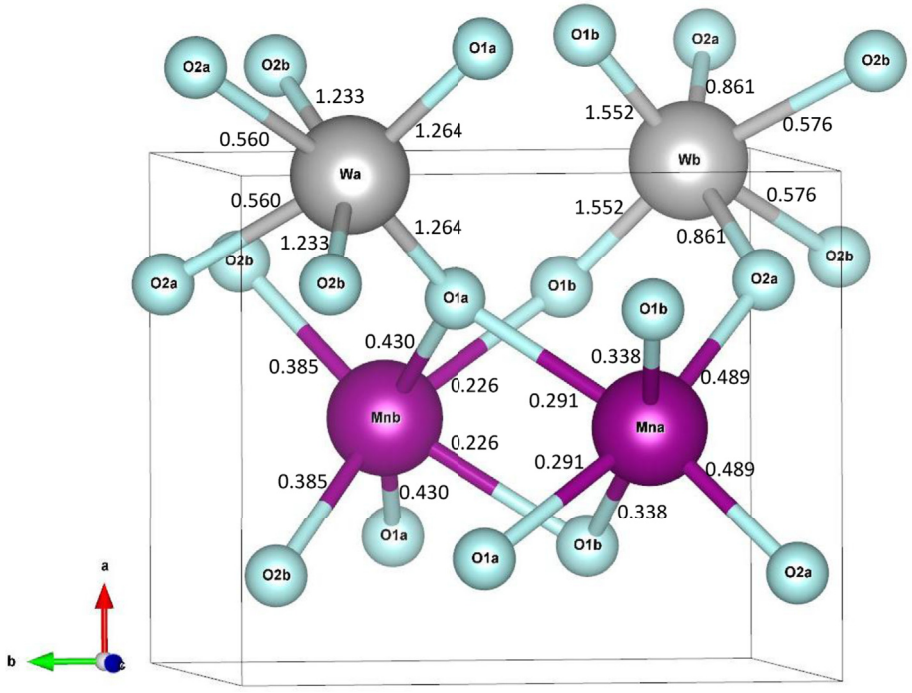

Fig. 1. Atomic sites in the unit cell of huebnerite ($MnWO_4$) at 10 K in the polar space group ***P*2**. Individual bond valence to oxygens are given to the independent sites for Mn^{2+} and W^{6+}.

JANA2006 [14]. The structure of AF2 was analysed according the magnetic superstructure space group formalism [15]. The representation of the magnetic structure has been made with the programme VESTA [16].

3. Results and discussion

3.1. The atomic structure of AF2

In accord with previous observation in Ref. [5], weak *h0l* reflections with l = odd were detected in NSCD at 10 K, as well. They are forbidden to the c-gliding plane perpendicular to the ***b*** axis in ***P*2/*c***. Therefore, the polar space group ***P*2** as the highest direct monoclinic subgroup of ***P*2/*c*** could be selected out to refine the atomic model of AF2. The refined parameters of the nuclear structure in AF2 are given in Table 2. Note that each pair of atoms which are named identically except for the subscripts, e.g. Mn_a and Mn_b, are symmetrically related to each other in ***P*2/*c*** but independent in ***P*2**. The unique site property of Mn_a distinguishable from Mn_b can be estimated by relative shifts of this atomic pair in ***P*2** from their average position in ***P*2/*c***, which is extremely small, as shown in Table 3. Hence, intrinsic dipole moments from such a hidden polar atomic arrangement might be too weak to be detected microscopically.

However, a strong indication of symmetry lowering from ***P*2/*c*** down to ***P*2** is revealed when considering bond valence sum values (*VBS*) [17]. For instances, *BVS* of Mn_aO_6 (= 2.236) is larger than *BVS* of Mn_bO_6 (= 2.162). As given in Table 4, the major difference of Mn_a from Mn_b is due to their bonding distances to the same oxygen site $O1_a$, i.e. $d(Mn_a\text{-}O1_a) = 2.247(6)$ Å > $d(Mn_b\text{-}O1_a) = 2.102(6)$ Å. For the case between W_aO_6 (*BVS* = 6.114) and W_bO_6 (*BVS* = 5.978), $d(W_a\text{-}O1_a) = 1.831(5)$ Å > $d(W_b\text{-}O1_a) = 1.754(5)$ Å. In Fig. 1, the degree of unique site character at four octahedral sites for Mn^{2+} and W^{6+} is demonstrated in terms of *BVS*. Similarly, we have observed a strong variation in occupancy parameters at two independent Mn_a and Mn_b sites in (In^{3+}, Na^{+})-doped $MnWO_4$ compounds [6]. In conclusion, magnetic Mn^{2+} cations occupy two different polar atomic sites within the polar nuclear structure of AF2. This is a relevant symmetric reason for the presence of two distinct chiral spin-textures, as described in the following section.

Table 1
Experimental and refinement parameters of neutron single crystal diffraction data of huebnerite at 10 K.

Compound	huebnerite ($MnWO_4$)
Crystal size	3.3 × 6.5 × 17.7 mm^3
Calculated density	7.3167 g/cm^3
Lattice parameters	a = 4.808(1) Å
	b = 5.742(1) Å
	c = 4.979(1) Å
	β = 91.03(1) °
	V = 137.44(5) $Å^3$
Space group of the atomistic structure	***P*2**
Magnetic superspace group	***P*21′(α ½ γ)0s**
Propagation vector ***k***	(−0.2152, 0.5, 0.4558)
Wavelength of neutron radiation	1.0481 Å
Monochromator	Cu(422)
Measuring temperature	10 K
Absorption coefficient	0.027 μm^{-1}
Maximal sin(θ)/λ observed	0.626
$2\theta_{min}$; $2\theta_{max}$	14.40°; 41.06°
h k l m range	−1 < h < 6;
	−7 < k < 7;
	−2 < l < 3;
	−1 < m < 1
Condition for unobserved reflections	I > 3 σ(I)
R for merging	4.10
Number of total and magnetic reflections after merging	628/103
R for against F for main reflection	5.60
wR for against F^2 for main reflections	10.83
R for against F for magnetic reflections	14.04
wR for against F^2 for magnetic reflections	20.01
Goodness-of-Fit (S)[a]	3.47
$Shift/\sigma_{max}$ $Shift/\sigma_{av}$	0.0500; 0.0143

$R = [\Sigma||Fo|-|Fc||/\Sigma|Fo|]$.
$wR = [\Sigma\, w(F_o^2-F_c^2)^2/\Sigma\, wF_c^2]^{1/2}$.
Weighting $w = 1/(\sigma^2(I) + 0.0004*I^2)$.
$S = [\Sigma\, w(F_o^2-F_c^2)^2/(m-n)]^{1/2}$, where F_o and F_c are observed and calculated structure factors, respectively, m is number of reflections, and n is number of parameters.
[a] There were no correlations larger than 0.9 in the last refinement cycle.

3.2. The magnetic structure at 10 K

The propagation vector ***k*** (−0.2152, 1/2, 0.4558) determined at 10 K

Table 2
Refined atomic parameters of the atomistic structure of $MnWO_4$ at 10 K in the polar space group ***P*2** with isotropic atomic displace parameter U_{iso} [Å^2].

Atomic Site	Atom type	Coordinate			Occupancy	U_{iso} [Å^2]
		x	y	z		
Mn_a	Mn	0.5	0.3194(10)	0	0.5	0.005(2)
Mn_b	Mn	0.5	0.6871(10)	0.5	0.5	0.005(2)
W_a	W	0	0.8194[a]	0	0.5	0.007(2)
W_b	W	0	0.1777(8)	0.5	0.5	0.001(2)
$O1_a$	O	−0.2520(7)	−0.3798(6)	−0.1566(16)	1	0.008(1)
$O1_b$	O	−0.2522(5)	−0.6306(5)	0.3692(17)	1	0.003(1)
$O2_a$	O	−0.2207(6)	0.1021(7)	−0.1815(19)	1	0.005(1)
$O2_b$	O	−0.2009(6)	−0.1025(7)	0.2978(19)	1	0.004(1)

[a] The coordinate y of the atomic site W_a was fixed in the entire refinement process to avoid the origin shift along the polar axis.

Table 3
Relative atomic shifts between the respective atom pairs in ***P*2** which would be equivalent to each other in ***P*2/*c*** (neutron single crystal data, 10 K).

Atom site pair	Δx	Δy	Δz
Mn_a-Mn_b	0	0.0065	0
W_a-W_b	0	0.0029	0
$O1_a$-$O1_b$	0.0002	0.0104	0.0258
$O2_a$-$O2_b$	0.0198	0.0004	0.0207

Table 4
Interatomic distance (*R*) between atomic site 1 and 2, single bond valence, and bond valence sum (*BVS*) in the atomic structure of huebnerite in ***P*2** at 100 K.

Site 1	Site 2	*R* (Å)	Bonding valence[a]	Site 1	Site 2	*R* (Å)	Bonding valence[a]
Mn_a	$O1_a$	2.247 (6)	0.291	Mn_b	$O1_a$	2.102(7)	0.430
	$O1_a$	2.247 (6)	0.291		$O1_a$	2.102(7)	0.430
	$O1_b$	2.191 (7)	0.338		$O1_b$	2.280(6)	0.226
	$O1_b$	2.191 (7)	0.338		$O1_b$	2.280(6)	0.226
	$O2_a$	2.054 (6)	0.489		$O2_b$	2.143(6)	0.385
	$O2_a$	2.054 (6)	0.489		$O2_b$	2.143(6)	0.385
	BVS	2.236			*BVS*	2.162	
W_a	$O1_a$	1.831(5)	1.264	W_b	$O1_b$	1.754(5)	1.552
	$O1_a$	1.831(5)	1.264		$O1_b$	1.754(5)	1.552
	$O2_a$	2.132(5)	0.560		$O2_a$	1.972(8)	0.861
	$O2_a$	2.132(5)	0.560		$O2_a$	1.972(8)	0.861
	$O2_b$	1.840(8)	1.233		$O2_b$	2.121(7)	0.576
	$O2_b$	1.840(8)	1.233		$O2_b$	2.121(7)	0.576
	BVS	6.114			*BVS*	5.978	
$O1_a$	Mn_a	2.247 (6)	0.291	$O1_b$	Mn_a	2.191 (7)	0.338
	Mn_b	2.102(7)	0.430		Mn_b	2.280(6)	0.226
	W_a	1.831(5)	1.264		W_b	1.754(5)	1.552
	BVS	1.985			*BVS*	2.156	
$O2_a$	Mn_a	2.054 (6)	0.489	$O2_b$	Mn_b	2.143(6)	0.385
	W_a	2.132(5)	0.560		W_a	1.840(8)	1.233
	W_b	1.972(8)	0.861		W_b	2.121(7)	0.576
	BVS	1.910			*BVS*	2.194	

BVS = exp{(R_0 − *R*)/b}.
Mn + 2 R_0 = 1.790; *b* = 0.370.
W+6 R_0 = 1.917; *b* = 0.370.
[a] Using the cation type-coordination number-charge-specific parameters R_0 and *b* given in Ref. [17], as follows.

is comparable to that given in literature [1,3,18,19]. The (3+1)-dim. magnetic superspace group ***P*2.1′(α1/2γ)0s** is the only subgroup of the paramagnetic group ***P*2.1′** compatible with the ***k*** vector [15], allowing electric polarisation magnetically induced in the crystallographic ***b*** direction, i.e. P_b [3,18–21]. Representative operations of ***P*2.1′(α,1/2,γ) 0s** is explicated in Table 5 with the identity (1) and the two-fold rotation in y (2_y) combined with time-inversion ('). A fourth element of 1/2 in Seitz-type notations represents internal translation along the modulation component x_4 for the time-inversion in 1′ and 2_y' [1]. The one-line magnetic superspace group symbol *s* stands for a translation of 1/2 in x_4 by operating 1' [15]. The magnetic moment is described by $M_j(x_4) = M_{j,cos}(\cos 2\pi \cdot n \cdot x_4) + M_{j,sin}(\sin 2\pi \cdot n \cdot x_4)$, where $x_4 = \boldsymbol{k}\cdot(\boldsymbol{r_j} + \boldsymbol{t})$ with the lattice translation ***t*** and the position vector $\boldsymbol{r_j}$ of the atom j in the 0th unit cell. It is important to emphasize that the magnitude of the magnetic moment at Mn_a is not necessary to be equal to that at Mn_b, i.e. $M(Mn_a) \neq M(Mn_b)$, because of their independence in this polar magnetic superspace group. Their maximal magnitudes are $M_{max}(Mn_a) = 4.0(5)\ \mu_B$ and $M_{max}(Mn_b) = 3.2(5)\ \mu_B$ (Table 6). However, the spin ellipses at Mn_a and Mn_b exhibit the same direction of chirality, as illustrated in Fig. 2.

In order to compare this new AF2 model to the previous model refined using the space group ***P*2/*c*** in the X-centering setting ***X*2.1′(α,0,γ) 0s** [1], a double unit cell along ***b*** was chosen with the new propagation vector ***k*'** (−0.2152, 0, 0.4558), having four Mn sites with constraints: $M(Mn1_a) = M(Mn2_a)$; $M(Mn1_b) = M(Mn2_b)$. The refined coefficients of magnetic moments in the X-centering setting are presented in Tables 6 and 7. The magnitudes of helical spin-waves at Mn_a and Mn_b differ from each other, which is independent on their atomic structure in ***P*2** [this study] and ***P*2/*c*** [1] due to the common polar magnetic space group. Nonetheless, the canting angles (α) of magnetic moments against the ***a*** axis in the (***a*-*c***) plane differ in both models, as shown in Table 7. A significant distinction between the magnetization at Mn_a and Mn_b in the easy axis (M_{easy}) and in the ***b*** axis (M_b) is found in the ***P*2** model. Consequently, their ellipticity (η) values, defined as the ratio M_b/M_{easy} [19–21], are very differ in the ***P*2** model, i.e. $\eta(Mn_a) = 0.92(6)$; $\eta(Mn_b) = 0.77(4)$. Their average value $\eta = 0.84$ is nearly equal to the ellipticity $\eta(Mn_a) = 0.80$ and $\eta(Mn_b) = 83$ evaluated with the ***P*2/*c*** model [1]. It turns out that the ellipticity as the order parameter for ferroelectricity magnetically induced [3,19–23] shows subtle difference in both models.

The bulk electric polarisation P_b ~34.5 μCm^{-2} in huebnerite at 10 K could be estimated according to P_b (T) = (21.8 μCm^{-2}K$^{-1/2}$)(T$_2$ − T)$^{1/2}$ [23], where T_2 is the magnetic phase transition from AF3 to AF2 (= 12.5 K [8]) and T = 10 K. For the ratio $P_b(Mn_a)/P_b(Mn_a)$ is directly proportional $M_{easy}M_b\sin\alpha(Mn_a)/M_{easy}M_b\sin\alpha(Mn_a) = 2.19$, we could estimate $P_b(Mn_a) = 22.8\ \mu Cm^{-2}$ and P_b (Mn_b) = 12.2 μCm^{-2} with our model for AF2. In following the microscopic model suggested by Katsura

Table 5
Representative operations of the magnetic superspace group ***P*2.1′** (α, 1/2, γ)0s. Generalized Seitz notation and symmetry cards used in Jana2006 are listed with the labels m (no time inversion) and -m (time inversion involved in the operation).

***P*2.1′(α,1/2,γ)0s**					
{1 | 0 0 0 0 }	x_1	x_2	x_3	x_4	m
{2_y | 0 0 0 1/2 }	- x_1	x_2	-x_3	x_2-x_4	m
{1' | 0 0 0 1/2 }	x_1	x_2	x_3	x_4+1/2	-m
{2_y' | 0 0 0 1/2 }	- x_1	x_2	-x_3	x_2-x_4+1/2	-m

Table 6
Coefficients describing the magnetic moment of the AF2 phase of huebnerite. M_{min} and M_{max} given in Bohr magnetons [μ_B] are the minimal and maximal magnetic moment magnitudes, respectively, within 100 × 100 × 100 unit cells for both primitive and X-centering settings.

	M^x_{cos}	M^y_{cos}	M^z_{cos}	M^x_{sin}	M^y_{sin}	M^z_{sin}	M_{min}	M_{max}
P2.1′ (α, 1/2, γ)0s								
Mn_a	−2.8(4)	1.9(1)	−1.9(1)	1.8(2)	3.0(2)	1.2(2)	3.5(3)	4.0(5)
Mn_b	2.3(4)	1.3(1)	1.3(3)	1.5(3)	−2.0(2)	0.9(2)	2.4(6)	3.2(5)
X2.1′ (α, 0, γ)0s								
Mn_a	0	3.6(2)	0	3.3(4)	0	2.2(2)	3.5(3)	4.0(5)
Mn_b	0	−2.4(2)	0	−2.8(4)	0	−1.6(3)	2.4(6)	3.2(5)

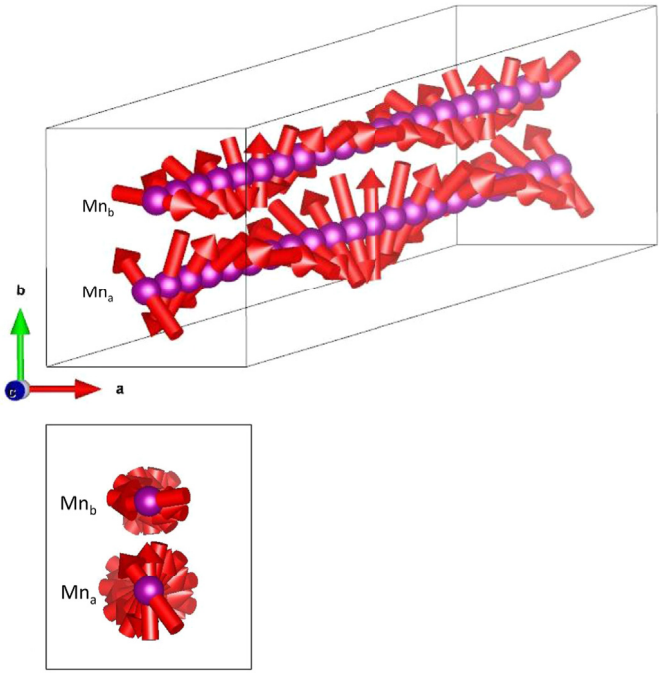

Fig. 2. Two different helical spin-waves in the multiferroic phase AF2 of huebnerite at 10 K in the polar superspace group ***P***2.1′ (α, 1/2, γ)0s based on the polar space group ***P***2. These two spin-textures are clearly seen on the projection parallel to the c axis at the bottom.

Table 7
Magnetic moment parameters in huebnerite at 10 K, obtained from structure refinements in ***P***2 using neutron single crystal data. A comparison is made with those values from a previous model refined using the non-polar space group ***P***2/*c* [1].

	α[°]	M_{easy}	M_b	Ellipticity η
P2				
X2.1′ (α, 0, γ)0s				
Mn_a	34.5(3)	4.0(5)	3.6(2)	0.92(6)
Mn_b	29.3(3)	3.2(5)	2.4(2)	0.77(4)
P2/*c*				
X2.1′ (α, 0, γ)0s				
Mn_a	37(2)	4.1(1)	3.26(7)	0.80
Mn_b	30(2)	3.6(1)	2.97(6)	0.83

et al. [24], $P_b(Mn_a)$ is connected with the vector product $[M(Mn_a) \times M(Mn_b)]$ along the ***c***-axis via a constant, $A(Mn_a)$; $P_b(Mn_b)$ is connected with the vector product $[M(Mn_b) \times M(Mn_a)]$ via another constant, $A(Mn_b)$. The constants $A(Mn_a)$ and $A(Mn_b)$ depend on the spin-orbit coupling and super-exchange interactions [19–24]. The calculated values for $A(Mn_a)$ and $A(Mn_b)$ are about 10 $\mu Cm^{-2}\mu_B^{-2}$ and 12 $\mu Cm^{-2}\mu_B^{-2}$, respectively, with the ***P***2 model. Hence, a relevant conclusion is drawn: the *ME* coupling arising from the transverse-helical spin ordering is strongly dictated by atomic site symmetry.

4. Conclusion

Neutron single-crystal diffraction data of huebnerite at 10 K was analysed based on the polar space group ***P***2, revealing the new model for AF2 in the (3+1)-dim. superspace symmetry ***P***2.1′ (α, 0, γ)0s.

The ellipticity at Mn_a and Mn_b estimated to be 0.92 and 0.77, respectively, indicate different contributions of two helical spin-waves to improper ferroelectricity. The site character difference between Mn_a and Mn_b is significant with respect to their bond valences to oxygens. The current study concludes that the true origin of the magnetoelectric properties observed in the title compound is the polar atomic arrangement. Weak intrinsic dipole moments can be microscopically detectable merely by the polar transverse-helical spin ordering.

Acknowledgement

SHP acknowledges German Federal Ministry of Education and Research (BMBF) for the financial support via 05K13WMB.

References

[1] I. Urcelay-Olabarria, J.M. Perez-Mato, J.L. Ribeiro, J.L. Garcia-Munoz, E. Ressouche, V. Skumryev, A.A. Mukhin, Phys. Rev. B 87 (2013) 014419.
[2] I.V. Solovyev, Phys. Rev. B 87 (2013) 144403.
[3] K. Taniguchi, N. Abe, H. Sagayama, S. Ohtani, T. Takenobu, Y. Iwasa, T. Arima, Phys. Rev. B 77 (2008) 064408.
[4] X. Zhang, Q. Liu, J.W. Luo, A.J. Freeman, A. Zunger, Nat. Phys. 10 (2014) 387–393.
[5] S.-H. Park, B. Mihailova, B. Pedersen, C. Paulmann, D. Behal, U. Gattermann, R. Hochleitner, J. Mag. Mag. Mater. 394 (2015) 160–172.
[6] U. Gattermann, S.-H. Park, C. Paulmann, G. Benka, C. Pfleiderer, J. Solid St. Chem. 244 (2016) 140–150.
[7] U. Gattermann, B. Roeska, C. Paulmann, S.-H. Park, J. Cryst. Growth 453 (2016) 40–48.
[8] U. Gattermann, G. Benka, A. Bauer, A. Senyshyn, S.-H. Park, J. Mag. Mag. Mater. 398 (2016) 167–173.
[9] U. Gattermann, S.-H. Park, M. Kaliwoda, J. Solid St. Chem. 219 (2014) 191–200.
[10] S.-H. Park, J. Schefer, B. Roeska, N. Holtgrewe, M. Ahart, to be submitted.
[11] B. Liu, S.-H. Park, D. Behal, B. Pedersen, A. Schneidewind, submitted.
[12] Heinz Maier-Leibnitz-Zentrum, et al., RESI: thermal neutron single crystal diffractometer, J. Large-Scale Res. Facil. 1 (2015), https://doi.org/10.17815/jlsrf-1-23. A4.
[13] A.M.M. Schreurs, X. Xian, L.M.J. Kroon-Batenburg, J. Appl. Cryst. 43 (2010) 72–80.
[14] V. Petricek, M. Dusek, L. Palatinus, Z. Krist. 229 (5) (2014) 345–352.
[15] J.M. Perez-Mato, J.L. Ribeiro, V. Petricek, M.I. Aroyo, J. Phys. Condens. Matter 24 (2012) 163201.
[16] K. Momma, F. Izumi, VESTA 3 for three-dimensional visualization of crystal, volumetric and morphology data, J. Appl. Crystallogr. 44 (2011) 1272–1276.
[17] I.D. Brown, D. Altermatt, Acta Cryst. B 41 (1985) 244–247.
[18] G. Lautenschläger, H. Weitzel, T. Vogt, R. Hock, A. Böhm, M. Bonnet, H. Fuess, Phy. Rev. B 48 (1993) 6087.
[19] K. Taniguchi, N. Abe, T. Takenobu, Y. Iwasa, T. Arima, Phys. Rev. Lett. 97 (2009) 097203.
[20] A.H. Arkenbout, T.T.M. Palstra, T. Siegrist, T. Kimura, Phys. Rev. B 74 (2006) 184431.
[21] H. Sagayama, K. Taniguchi, N. Abe, T.-H. Arima, M. Soda, M. Matsuura, K. Hirota, Phys. Rev. B 77 (2008) 220407.
[22] Y. Yamasaki, H. Sagayama, T. Goto, M. Matsuura, K. Hirota, T. Arima, Y. Tokura, Phys. Rev. Lett. 98 (2007) 147204.
[23] P. Tolédano, B. Mettout, W. Schranz, G. Krexner, J. Phys. Condens. Matter 22 (2010) 065901.
[24] H. Katsura, N. Nagaosa, A.V. Balasky, Phys. Rev. Lett. 95 (2005) 057205.